Research Article | Vol. 30, No. 6 / 14 Mar 2022 / Optics Express 10071
Optics EXPRESS

Feedback control of atom trajectories in a horizontal atom gravity gradiometer

LEI ZHU,[1] JIAQI ZHONG,[1,2,3] XIAOWEI ZHANG,[1] WEI LYU,[2] WU LIU,[2] WEIHAO XU,[2] XI CHEN,[1,2] JIN WANG,[1,2,4] AND MINGSHENG ZHAN[1,2,5]

[1]*State Key Laboratory of Magnetic Resonance and Atomic and Molecular Physics, Innovation Academy for Precision Measurement Science and Technology, Chinese Academy of Sciences, Wuhan 430071, China*
[2]*School of Physical Sciences, University of Chinese Academy of Sciences, Beijing 100049, China*
[3]*jqzhong@wipm.ac.cn*
[4]*wangjin@apm.ac.cn*
[5]*mszhan@apm.ac.cn*

Abstract: The coincidence between the atom trajectory and the Raman pulse sequence is very important for an intersection type atom interferometer. Here we present a feedback control technique for the atom trajectories in our horizontal gravity gradiometer, which improves the stabilities of the trajectories by about 2 orders of magnitude. Through the further study of the dependence of the interferometer contrasts on the atom trajectories, we lock the trajectories at optimal positions. And by this technique, the sensitivity of the gravity gradiometer is improved from 982 E/Hz$^{1/2}$ to 763 E/Hz$^{1/2}$, while the long-term stability is enhanced more significantly and reaches 8.9 E after an integration time of 6000 s. This work may provide hints to other experiments based on intersection type atom interferometers.

1. Introduction

As a new type of sensor based on quantum technology, atom interferometry using stimulated Raman transitions has very broad application prospects in precision measurement. According to the spatial configuration between the Raman laser beams and the atom trajectory, the atom interferometers (AIs) can be divided into two types, the full coverage type and the intersection type. In the former type of AIs, the entire atom trajectory is covered by Raman laser beams, atoms can see the light whenever the Raman laser is pulsed on. The full coverage AIs can serve as gravimeters [1–9] and vertical gravity gradiometers [10–14]. In the later type of AIs, the Raman laser beams intersect the atom trajectory at angles, and the photons can only interact with atoms at specific time-space points. Thereby, atom gyroscopes [15–20] and horizontal gravity gradiometers [21] belong to the intersection type AIs.

In principle, due to the Gaussian distribution of the transverse light intensity, the atoms' effective Rabi frequency varies with their position relative to the Raman laser beam. Therefore, to an intersection type AI, the coincidence between the atom trajectory and the time sequence of Raman laser pulses yields the highest contrast of interferometer signal. However, the initial position of the atom cloud is susceptible to the deterioration of the intensity balance of trapping lasers and the drift of the magnetic field, resulting in the fluctuation of the atom trajectory. The mismatch between the trajectory and the Raman pulse sequence reduces the fringe contrast and amplifies amplitude noise. Additionally, when the intensity ratio of the different components in the Raman laser is not completely optimized, the trajectory fluctuations will produce corresponding phase fluctuations to the interferometer signals via ac-Stark shift. Especially to the horizontal gravity gradiometers and gyroscopes, where two AIs share a common series of Raman laser pulses, asynchronous drifts of the two atom trajectories will decrease the grade of common mode noise rejection and produce measurement errors. Static calibration of atomic trajectories has

#450276 https://doi.org/10.1364/OE.450276
Journal © 2022 Received 6 Dec 2021; revised 2 Mar 2022; accepted 2 Mar 2022; published 11 Mar 2022

Optics EXPRESS

been implemented in an atom gyroscope [18], however, to our knowledge, the real-time feedback of atom trajectories has not been reported yet, which is very important in unquiet environment, especially for dynamic application scenarios.

Here, we present our new results on atom trajectory control in a horizontal atom gravity gradiometer. Firstly, we investigate the vertical trajectory drifts of the two atom fountains in our horizontal gravity gradiometer by the time of flight (TOF) signals, and demonstrate a new method of feed-back control of the trajectories by the manipulation of the environmental magnetic fields. Then we further study the relationships between the trajectory deviations and the interferometer contrasts, and lock the trajectories at optimal positions. This technique significantly improves the stabilities of the trajectories, thus both the sensitivity and the long-term stability of the gravity gradiometer are enhanced remarkably.

2. Atom gravity gradiometer

Our gravity gradiometer consists of two horizontally separated AIs. Two clouds of cold ^{85}Rb atoms are simultaneously trapped and launched upward on two parabolic trajectories. Two Raman laser beams propagate in the horizontal direction in the plane defined by the two atom trajectories, and the upper beam is coaxial with the line connecting the two apogees. Three Raman pulses characterized as Ω_{eff} τ=π/2, π and π/2 respectively (Ω_{eff} is the Rabi frequency and τ is the pulse duration), are applied on the two atom clouds and drive coherent Rabi oscillations between the $F = 2$ and $F = 3$ hyperfine ground states. The first Raman pulse is turned on when the atoms ascend to the position of the lower beam. For atoms initially populated in $F = 3$ state, this π/2 pulse leaves atoms in an equal superposition of $F = 2$ and $F = 3$ states, analogous to an optical beam splitter. When the atoms arrive the apex of the trajectories, the second Raman π pulse is turned on and transfer atoms in $F = 2$ entirely to $F = 3$ and vice versa, corresponding to a mirror. Finally, the gravitational force pulls the atoms back to the position of the lower Raman beam, and the last π/2 pulse redistributes the atomic populations in the two ground states thus completes Mach-Zehnder style atom interferometers. As the output of one AI, the population probability in the original hyperfine state $F = 3$ is given by $P = (1\text{-}\cos(\varphi_0+\varphi_g))/2$, where $\varphi_g = k_{\text{eff}} \cdot g T^2$ is the phase shift caused by local gravitational acceleration g, for T is the time intervals between the laser pulses and k_{eff} is the effective wave vector. And similarly, in the other AI, $\varphi_g{}' = k_{\text{eff}} \cdot g' T^2$. Given the horizontal distance of the two AIs L, we can get the horizontal gravity gradient

$$\Gamma_{\text{h}} = (g - g')/L = \Delta\varphi_g/(k_{\text{eff}} L T^2). \tag{1}$$

The differential phase shift caused by the gravity gradient $\Delta\varphi_g = (\varphi_g\text{-}\varphi_g{}')$ is extracted by the method of ellipse fitting [22]. For two cosine signals with definite phase difference $P_1 = (1\text{-}\cos(\varphi))/2$, $P_2 = (1\text{-}\cos(\varphi+\Delta\varphi))/2$, the relation between the two signals can be expressed by ellipse equation

$$AP_1^2 + BP_1P_2 + CP_2^2 + DP_1 + EP_2 + F = 0. \tag{2}$$

The parameters A, B, C, D, E, F can be obtained by the least squares fitting, and the differential phase is

$$\Delta\varphi = \cos^{-1}(-B/2\sqrt{AC}). \tag{3}$$

By this method, the differential phase can be directly extracted, while the common mode phase noise in the two signals is significantly rejected.

The detailed scheme is shown in Fig. 1 and Fig. 2. ^{85}Rb atoms are pre-cooled in two-dimensional magneto-optical traps (2D-MOTs) and loaded to three-dimensional magneto-optical traps (3D-MOTs). After polarization-gradient cooling (PGC), about 5×10^8 atoms in $F = 3$ states with the temperature around 4.5 μK are prepared in each AI. Then the atoms are launched upward by (0, 0, 1) type moving molasses, the initial velocities are 2.05 m/s, correspond to the fountain heights of about 22 cm above the 3D-MOTs. After 37.5 ms, atoms ascend to the position about

Optics EXPRESS

7 cm above 3D-MOTs, horizontal bias magnetic fields are switched on to eliminate the degeneracy of the magnetic sublevels and defines the quantization axis, then a microwave π pulse and a succeeding resonant laser pulse is applied to transfer the atoms in $|F=3, m_F=0>$ state to $|F=2, m_F=0>$ state and remove the residual atoms in $|F=3, m_F\neq 0>$ states. The magneto-insensitive atoms keep moving upward to the Raman interaction regions, where the vacuum chambers of the two interferometers are connected as one by a vacuum tube of rectangular cross-section with internal dimensions of 3 cm×18 cm×94.5 cm, three Raman pulses with the time intervals 114 ms and durations 6 μs (π/2), 12 μs (π) and 6 μs (π/2), respectively, are turned on successively when the atoms arrive at the intersections. 20.7 ms after the interference stage, atoms fall back through the detection region. The populations in $F=3$ and $F=2$ states are detected by two successive detection beams and the fluorescence in two AIs are fed into four photodiodes (PDs) respectively. Finally, we get the normalized population in two AIs

$$P_1 = \frac{S_{1,\,F=3}}{S_{1,\,F=3} + \alpha_1 S_{1,\,F=2}},\ P_2 = \frac{S_{2,\,F=3}}{S_{2,\,F=3} + \alpha_2 S_{2,\,F=2}}, \tag{4}$$

where $S_{i,F=j}$ denotes the fluorescence signal amplitudes of $F=j$ state in ith AI, α_i is the correction coefficient in ith AI due to different detection efficiencies between $F=3$ and $F=2$ states.

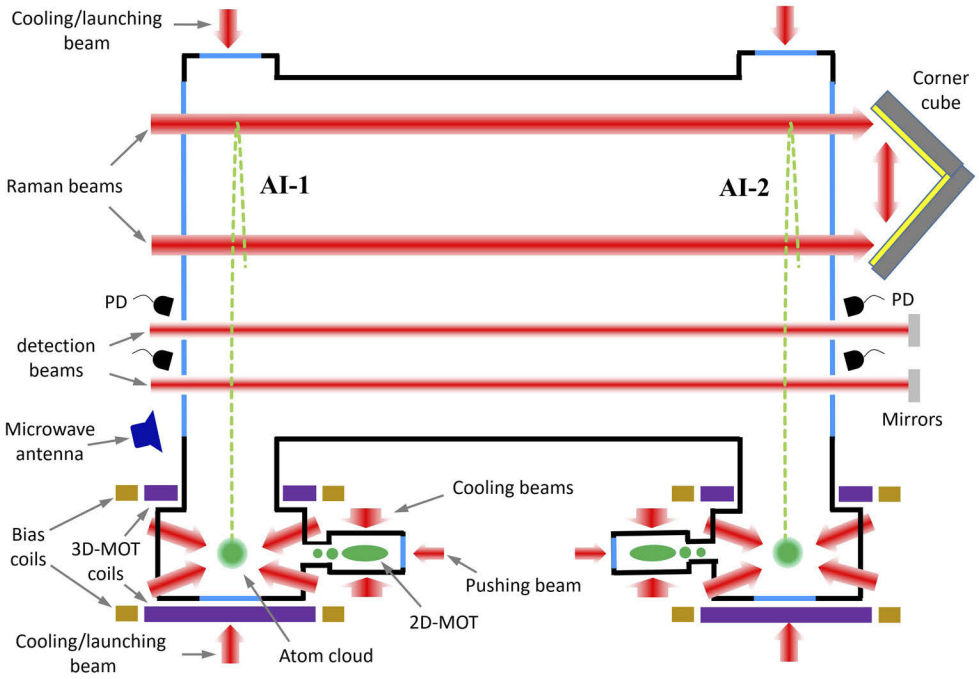

Fig. 1. Schematic diagram of the horizontal atom gravity gradiometer. The setup consists of two identical AIs with a horizontal separation. Two groups of ^{85}Rb atoms are trapped, launched, coherently manipulated, and finally detected synchronously. The gravity gradient is evaluated from the differential interferometer phase of the two AIs.

Here is an interesting phenomenon worth mentioning. To eliminate the effect of laser beam steering between the two AIs due to imperfect shapes of glass windows and the phase delay fluctuation caused by air density variation [23], the vacuum chamber for two AIs is designed as an integrated configuration with internal connection at the Raman interaction regions. Since in exception of the optical windows and the commercial valves, the vacuum chamber is entirely made of titanium, this inter-connection configuration makes it serve as a big waveguide at the

Optics EXPRESS

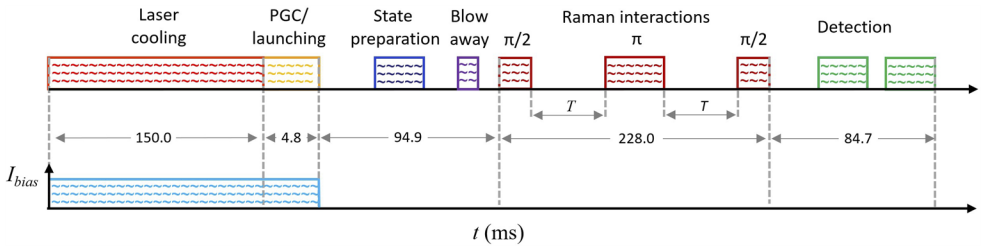

Fig. 2. Measurement sequence of the gravity gradiometer. I_{bias} is the current of the bias coils depicted in Sec. 4 for atom trajectory manipulation.

stage of initial-state preparation when the microwave π pulse is applied. As a result, only one microwave unit is needed to realize the initial-state preparation in both AIs, atoms in two sides can execute synchronous Rabi oscillations when the position and orientation of the antenna are carefully adjusted. The signals of two AIs' synchronous Rabi oscillations driven by a 1 W microwave are shown in Fig. 3.

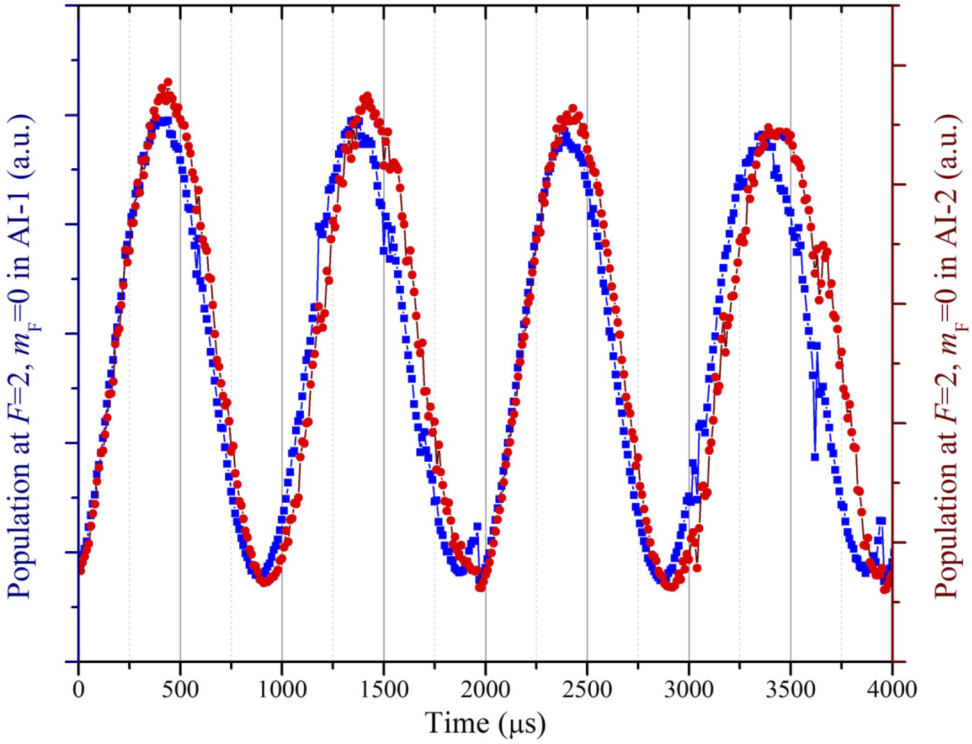

Fig. 3. Synchronous Rabi oscillations in dual AIs driven by only one microwave unit.

In our condition of almost no horizontal Doppler shift, the two-photon Raman transitions can only be excited by two lasers with the frequency difference equal to the hyperfine splitting between the two ground states, here for ^{85}Rb atoms it is 3.035733 GHz. And to perform gravity measurement, the Doppler-free transitions must be avoided. In our gravity gradiometer, as depicted in Fig. 4, the two lasers are generated by two optical paths from a same source, and each path contains an electro-optic modulator (EOM) in series with a double-passed acousto-optic

Optics EXPRESS

modulator (AOM). A microwave source with the frequency of 3.033733 GHz, 2 MHz lower than the hyperfine splitting, is employed to alternatively drive one of the two EOMs, and two RF signals with the frequencies 80 MHz and 79 MHz, respectively, are employed also to alternatively drive the two AOMs. Since the switches are controlled by same series of TTLs, the 2 MHz detuning of the microwave frequency can be compensated by the frequency difference 2×(80-79) MHz all the time. That makes the frequency difference between the two lasers (the +1 order sideband from EOM and the other non-EO-modulation carrier) matches the hyperfine splitting between the two ground states, while the Doppler-free transitions are avoided. A PLX corner cube reflector is utilized to guarantee the parallelism of the two beam levels to within 5 μrad, which is essential for good interferometer contrast, and the above switching scheme can keep the direction of the wave vector unchanged between π/2 and π Raman pulses.

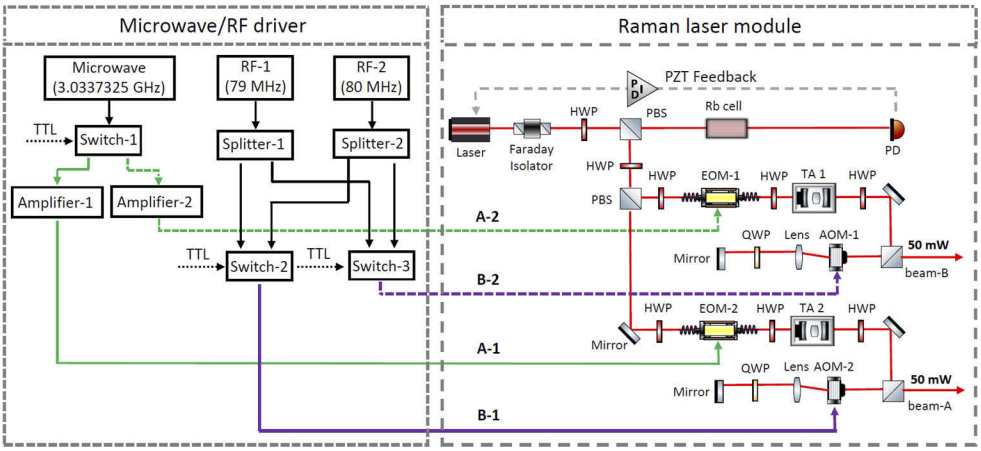

Fig. 4. The Raman laser system for the horizontal gravity gradiometer. (HWP: half-wave plate, PBS: polarization beam splitter, PD: photo detector, EOM: electro-optic modulator, TA: tapered amplifier, QWP: quarter-wave plate, AOM: acousto-optic modulator.)

3. Vertical trajectory drifts

As is mentioned above, to intersection type AIs, the mismatch between the trajectories and the time sequence of Raman laser pulses will probably reduce the contrast, brings amplitude noise and measurement errors into the interferometer signals. Here we present a measurement of the vertical drifts of the atom trajectories in our gravity gradiometer by the time of flight (TOF) signals. Without state preparation and Raman interaction, the atoms in fountains are directly excited by a detection laser pulse 134.7 ms after reaching the apexes. The pulse duration is set to 31.5 ms, so that the entire TOF fluorescence signal could be recorded by the PDs. A typical TOF signal pair is shown in Fig. 5, each trace contains data of 30 ms, we fitted the traces with Gaussian function and obtained the arrival times t_1 and t_2 corresponding to the maximum fluorescence intensities. A long-term measurement for about 20 hours was performed, the time domain data and corresponding Allan deviation for t_1 and t_2 are shown in Fig. 6. The P-V fluctuations of t_1 and t_2 are 1.4 ms and 1.7 ms respectively, while the Allan deviations start to warp up from the averaging time 20 s and ascend to the magnitude of 0.1 ms after 10^4 s of integration. Since the fluctuations are mainly caused by the vertical drifts of initial position of atom clouds, given the vertical velocity ~1.35 m/s at the detection region, the fluctuations of t_1 and t_2 correspond to the vertical position drifts of 1.9 mm and 2.3 mm respectively.

Optics EXPRESS

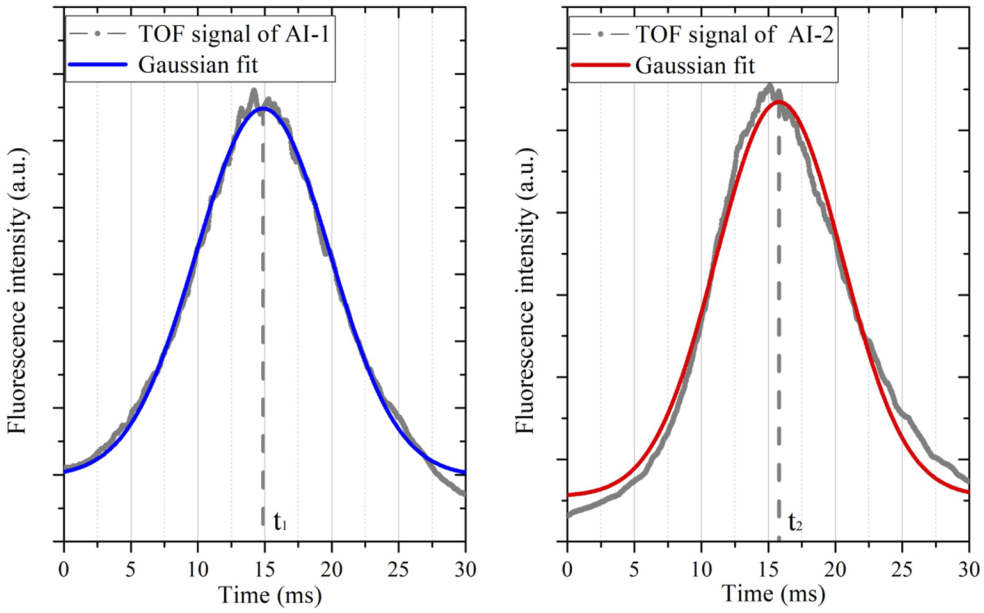

Fig. 5. Typical TOF signals in two AIs. The arrival times t_1 and t_2 are extracted from Gaussian fitting.

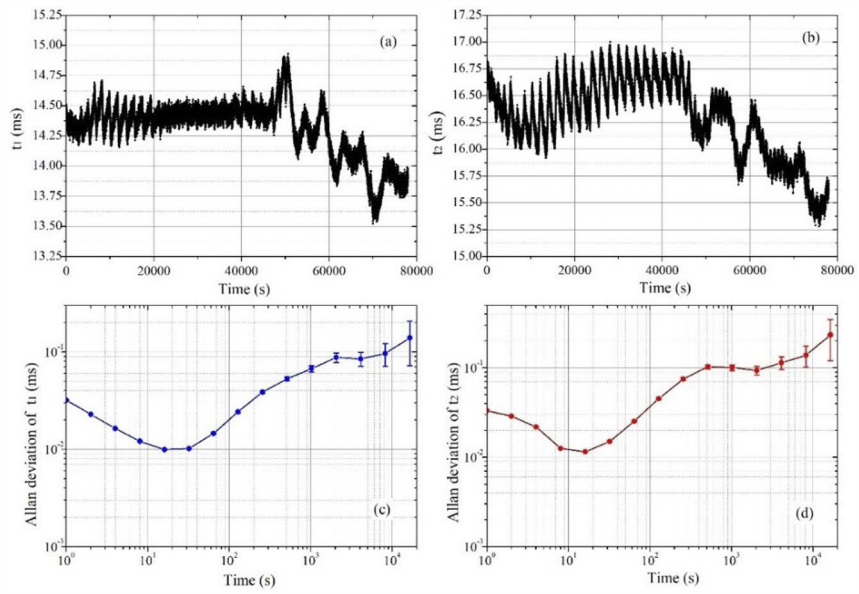

Fig. 6. Long-term measurements of the atoms' arrival times in two AIs (a, b) and the corresponding Allan deviations (c, d). The measurement time is about 20 hours with the sampling rate of 1 Hz.

Optics EXPRESS

4. Feedback control of the atom trajectories

The degradations of the intensity balance of trapping lasers and the drifts of the magnetic fields are the main reasons for the fluctuations of the initial vertical positions of the atom clouds. This can be alleviated by improving the stabilities of light intensities and internal magnetic fields. However, under the scene of drastic changes of the environmental parameters during mobile exploration in the field, this problem will again become serious. Therefore, we developed a technique to implement a feedback control of the vertical trajectory of atoms by additional modulation of bias magnetic field during the laser trapping phase.

As is shown in Fig. 1, in each AI, a pair of additional bias field coils is wound on the outside of the 3D-MOT anti-Helmholtz coils and is switched on during the stage of laser trapping and moving molasses. We scanned the driving currents of the two coil pairs, and recorded the arrival times t_1 and t_2. From the result shown in Fig. 7, we can see a very good linear relationship. By simple fitting, the slope coefficients are determined as 0.18 ms/mA and 0.19 ms/mA for the two AIs respectively.

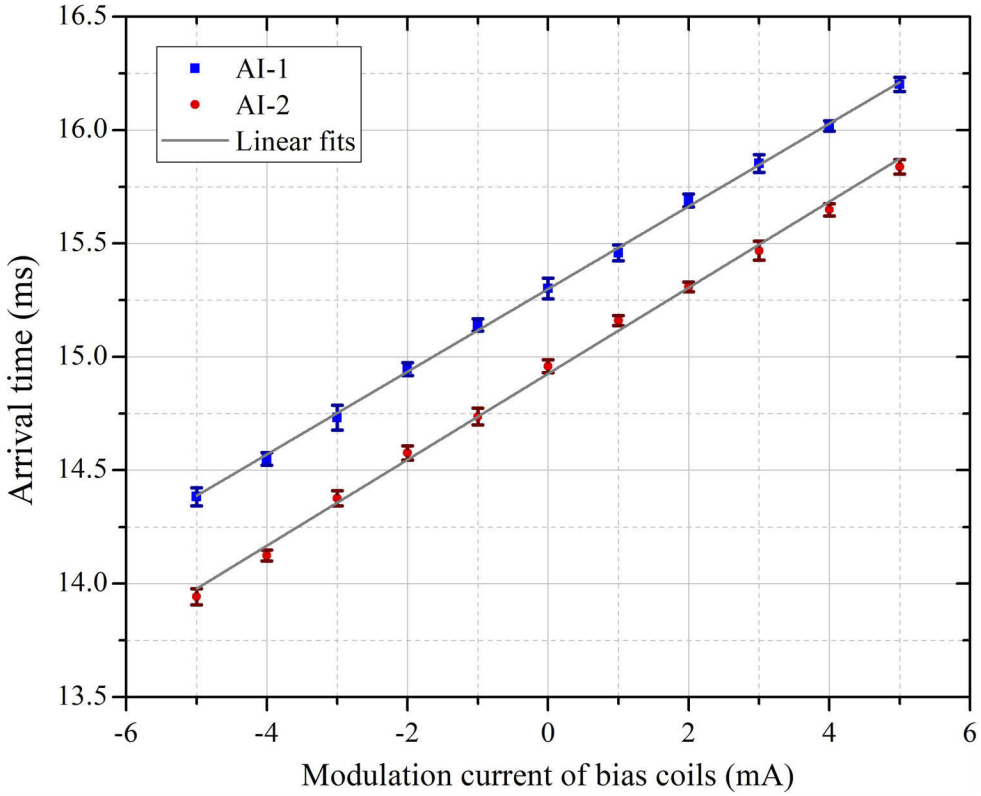

Fig. 7. Relations between the arrival times and the currents of the bias coils. All the datapoints come from ten scans of bias current and each scan takes about 6 s.

Based on the linear relationship above, we programmed a feedback control operation. The arrival times are recorded from shot to shot, and according to the average values, the feedback currents are refreshed every 20 s. This refresh rate is determined by the drift period of the trajectories, which induce upwarps in the Allan deviations, shown in Fig. 6, from the averaging time of around 20 s. To test the program, both locking points of t_1 and t_2 are set to 14 ms and another long-term measurement for about 6 hours are performed. The closed-loop results of time domain arrival times, corresponding Allan deviations and the feedback currents are shown in

Optics EXPRESS

Fig. 8. In these figures, no visible drift of arrival times is observed, the Allan deviations start to decrease from 20 s according to $1/\tau^{1/2}$ function and reach the level of about 2 μs after 4000 s integration, which corresponds to a trajectory stability of 2.7 μm. In comparison with the results in Fig. 6, long-term stabilities of the trajectories in both AIs are improved by about 2 orders of magnitude.

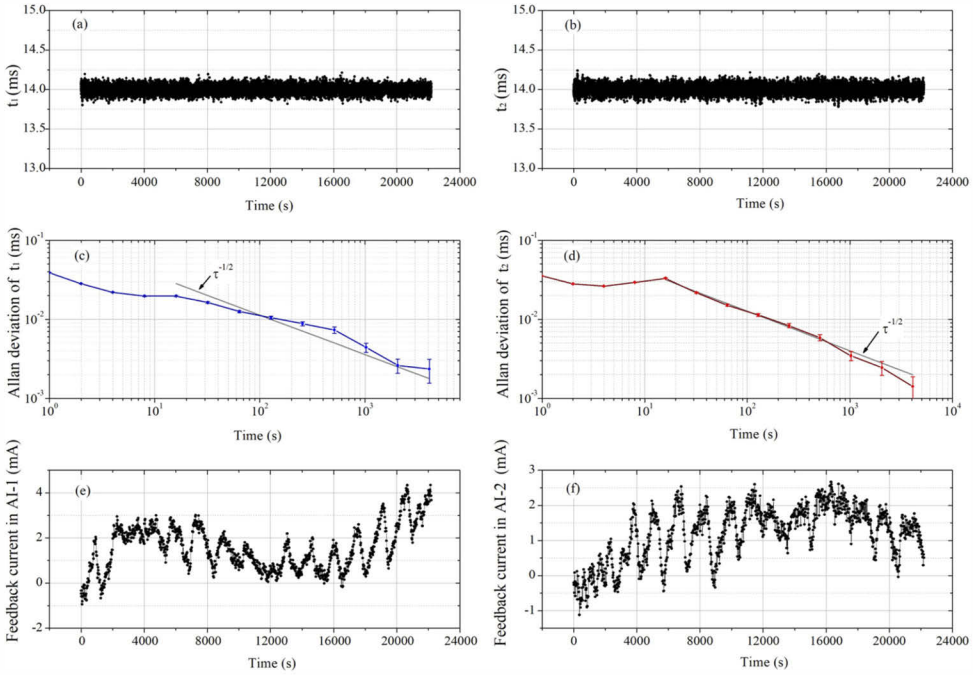

Fig. 8. Closed-looped arrival times in two AIs (a, b) and the corresponding Allan deviations (c, d). The long-term stabilities could reach the levels of 2 μs, corresponds to a trajectory stability of 2.7 μm. The drifts of the arrival times in Fig. 6 transfer to the feedback current of the bias coils (e, f).

5. Dependence of interferometer contrasts on atom trajectories

In an ideal Mach-Zehnder AI with all the atoms manipulated by a uniform and constant Raman light field, if the effective Rabi frequency Ω_{eff} and the π/2 pulse duration τ satisfy

$$2\Omega_{\text{eff}}\tau = \pi, \tag{5}$$

the probability of finding the atoms in the excited state is,

$$P_{\text{ideal}} = [1 - \cos(\varphi_1 - 2\varphi_2 + \varphi_3)]/2, \tag{6}$$

where φ_i is the phase of ith Raman laser pulse. In this case, the contrast of the interferometer fringes is 100%.

In an AI where atoms manipulated by three Raman laser pulses with varying intensities while the pulse durations are kept at τ, 2τ and τ. Given that Ω_0 is the reference Rabi frequency satisfies $2\Omega_0\tau=\pi$, and the Rabi frequencies of three pulses are $\Omega_1 = r_1\Omega_0$, $\Omega_2 = r_2\Omega_0$ and $\Omega_3 = r_3\Omega_0$,

Optics EXPRESS

respectively, then the probability of finding the atoms in the excited state is,

$$P_{\text{practical}} = \frac{1}{2}\left\{1 - \cos\left[\frac{(r_1 + 2r_2)\pi}{2}\right]\cos\left(\frac{r_3\pi}{2}\right) + \sin\left[\frac{(r_1 + 2r_2)\pi}{2}\right]\sin\left(\frac{r_3\pi}{2}\right)\cos(\varphi_1 - 2\varphi_2 + \varphi_3)\right\}. \tag{7}$$

Thus, the interferometer contrast becomes,

$$C = \frac{|\sin[(r_1 + 2r_2)\pi/2]\sin(r_3\pi/2)|}{1 - \cos[(r_1 + 2r_2)\pi/2]\cos(r_3\pi/2)}. \tag{8}$$

In most AIs, the transverse intensity distributions of Raman laser beams are Gaussian, expressed as

$$|E| = E_0 \exp\left[-\frac{r^2}{\omega_0^2}\right]. \tag{9}$$

Therefore, in our intersection type AIs, as depicted in Fig. 9, when the Raman lasers are pulsed on with referenced sequences, the drift of the vertical trajectory of the atoms will result in position deviations Δz from the center of the laser beams, and consequently lead to equivalent laser intensity decreases. Given that the size of our Raman laser beams $\omega_0 = 7.5$ mm, we simulated the relationship between the contrast and the transverse position deviation according to Eqs. (8) and (9). As shown in Fig. 9 (c), referring to a completely optimized time-space configuration, a vertical trajectory deviation of 2 mm corresponds to a theoretical reduction of interferometer contrast to about 70.8%. Especially for AIs originally with imperfect time-space configuration, an additional deviation with same value (i.e., from 1 mm to 3 mm) will result in an even drastic degradation.

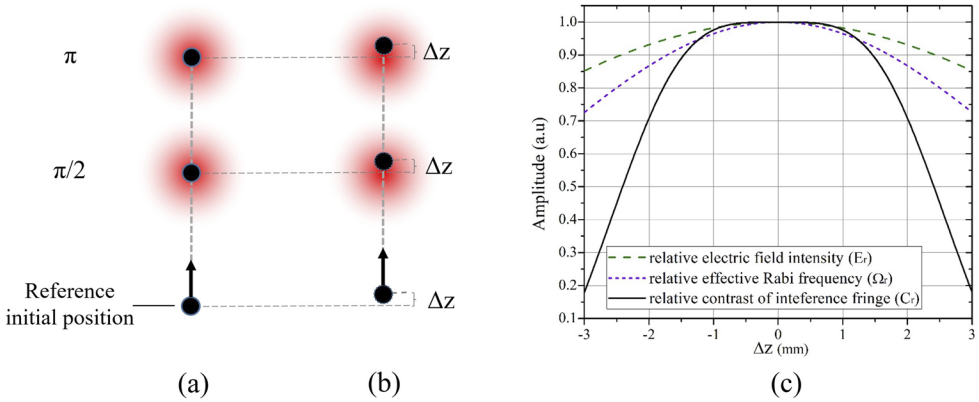

Fig. 9. Theoretical dependence of the interferometer contrast on the deviation of vertical atom trajectory. (a) and (b) depict the vertical deviation of atom trajectory, which results in a decrease of the light intensity interacting with the atoms. The solid line in (c) illustrates the theoretical degradation of interferometer contrast due to the deviation Δz, the contours of the Gaussian light field intensity and Rabi frequency are also shown as reference.

Based on the technique demonstrated in sect. 4, we experimentally investigated the dependence of interferometer contrasts on vertical atom trajectories in our horizontal gravity gradiometer. The arrival times t_1 and t_2 are locked and scanned from 13.50 ms to 16.17 ms with a step of 0.33 ms, the contrasts of both interferometers corresponding to each arrival time are measured and shown in Fig. 10. Within 2.67-ms scanning span, corresponds to 3.6-mm modulation range of atom trajectory, the contrasts vary up to 5%~6%. By Gaussian fitting, we obtained the maximum contrasts of the two interferometers as 27.1% and 22.7%, and the corresponding $t_1{}^\circ$ and $t_2{}^\circ$ are

Optics EXPRESS

14.1 ms and 15.7 ms respectively. The 1.6 ms difference between $t_1{}^\circ$ and $t_2{}^\circ$ is mainly caused by the TOF fitting error of the second interferometer, as shown in Fig. 5, a slight asymmetry of the signal results in a positive offset between the fitted profile center and the t_2 corresponds to the actual peak.

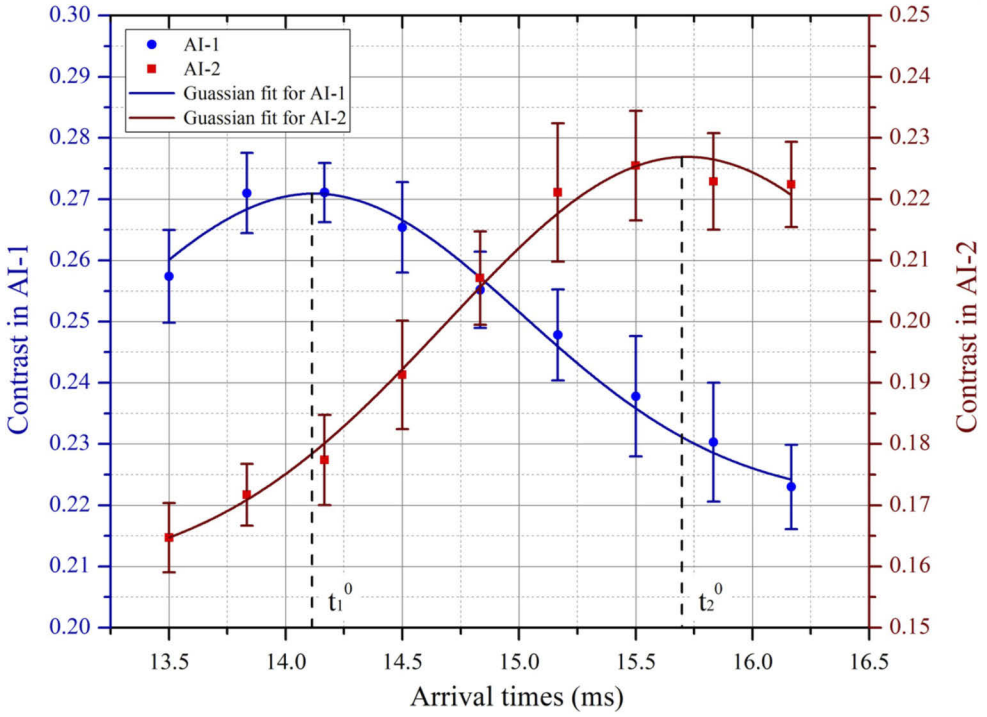

Fig. 10. Experimental dependence of interferometer contrasts on arrival times of atoms. Considering the Gaussian spatial distribution of atoms, these data are also fitted by Gaussian functions.

6. Application of the feedback control to the gravity gradiometer

In atom interferometers, the amplitude noise and detection noise will convert to phase noises in phase extraction. For certain amounts of amplitude and detection noises, the amplitude of converted phase noise is inversely proportional to the interferometer contrast. The feedback control of the atom trajectories will help to optimize the contrast and improve the stability, thereby reduce the phase noise. To test the effect of this technique, we compared the performances of our horizontal gravity gradiometer with and without the feedback loop.

In our gradiometer, the distance between the two AIs $L = 1.0$ m, and the time intervals between the laser pulses $T = 114$ ms, according to Eq. (1), the relationship between the deviation of gravity gradient and that of differential phase is

$$\sigma_\Gamma = 0.00478 \cdot \sigma_\varphi, \tag{10}$$

where 1 mrad corresponds to 4.78 E. One measurement process takes 580 ms, including 155 ms for laser cooling, 95 ms for state preparation, 228 ms for Raman interaction and 85 ms for detection. The differential phase is extracted by ellipse fitting every 40 measurements, and in trajectories closed-loop mode, one feedback operation is performed every 15 measurements. Since the drift of the trajectory is a slow process, these intermittent feedbacks could produce almost the same

Optics EXPRESS

effect as continuous feedbacks. Due to the high sensitivity to accelerations and the absence of vibration isolation devices, the fringes of single AI are completely submerged in the noise, whereas the differential ellipse between the two AIs maintains a high signal-to-noise ratio thanks to the mechanism of common mode rejection.

From the Allan deviations of the gravity gradiometer shown in Fig. 11, the sensitivity of the gradiometer is improved from 982 E/Hz$^{1/2}$ to 763 E/Hz$^{1/2}$ with the feedback loops. At the same time, due to the rejection of unsynchronized drifts of the two atom trajectories, the long-term stability is also improved, the measurement resolution reaches 8.9 E after 6000 s integration. In additional test of gravity field modulation, 850 kg lead bricks reciprocate in the center and side of the gradiometer, three sets of measurements are performed in each position and each set takes 10 min. As shown in Fig. 12, the variation of horizontal gravity gradient is measured to be 188 ± 11 E, which is in accordance with theoretical prediction 205 ± 9 E.

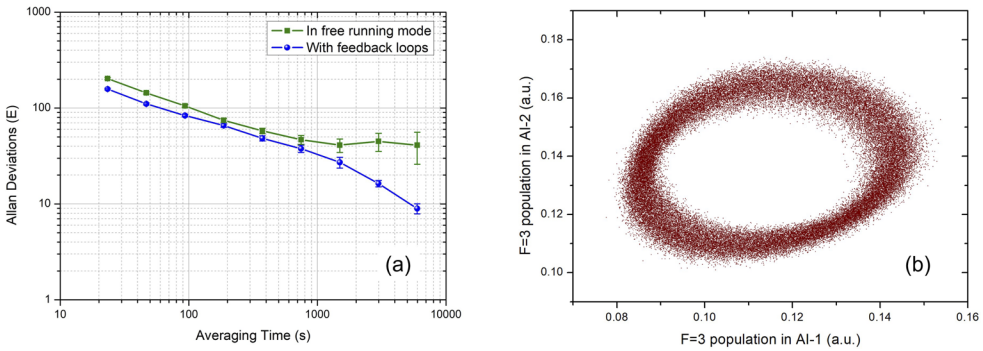

Fig. 11. (a) Comparison between the Allan deviations with and without the feedback loops. (b) Interferometer signals of the two AIs in differential mode, the ellipse contains approximately 60000 data of measurements.

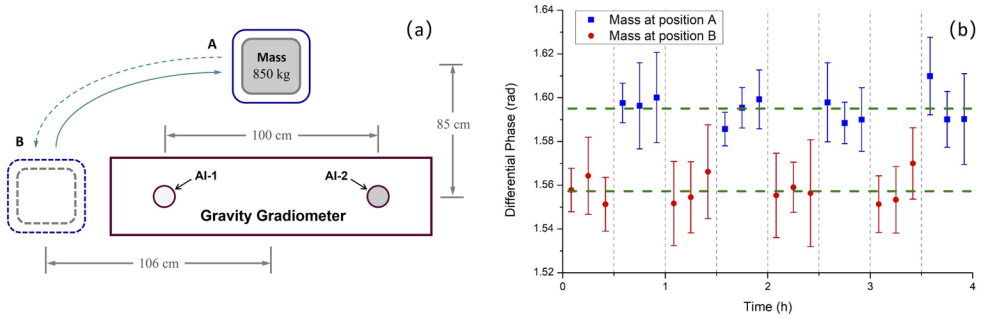

Fig. 12. The experiment of gravity field modulation. (a) is the top view of the arrangement schematic diagram. (b) shows the measured ellipse phase variation between the cases when the mass is at position A and position B. The averaged phase difference is 36.9 ± 2.1 mrad, corresponds to a gravity gradient variation 188 ± 11 E.

7. Conclusions

We have developed a horizontal gravity gradiometer based on dual AIs and realized a feedback control of the atom trajectories by the manipulation of the environmental magnetic fields. The drifts of the trajectories were initially observed to be up to 2 mm, and is suppressed by about 2 orders of magnitude through this technique. Subsequently, we studied the dependence

Optics EXPRESS

of interferometer contrasts on the vertical trajectories and locked the trajectories at optimal positions. Thus, the sensitivity of the gravity gradiometer was improved from 982 E/Hz$^{1/2}$ to 763 E/Hz$^{1/2}$, while the long-term stability was enhanced more significantly and reaches 8.9 E after an integration time of 6000 s. This work may provide hints to other experiments based on intersection type atom interferometers.

Funding. National Natural Science Foundation of China (91536221, 91736311).

Acknowledgments. We acknowledge the support from the China National Precise Gravity Measurement Facility.

Disclosures. The authors declare no conflicts of interest.

Data availability. Data underlying the results presented in this paper are not publicly available at this time but may be obtained from the authors upon reasonable request.

References

1. A. Peters, K. Y. Chung, and S. Chu, "Measurement of gravitational acceleration by dropping atoms," Nature **400**(6747), 849–852 (1999).
2. Z. K. Hu, B. L. Sun, X. C. Duan, M. K. Zhou, L. L. Chen, S. Zhan, Q. Z. Zhang, and J. Luo, "Demonstration of an ultrahigh-sensitivity atom-interferometry absolute gravimeter," Phys. Rev. A **88**(4), 043610 (2013).
3. T. Farah, P. Gillot, B. Cheng, A. Landragin, S. Merlet, and F. P. Dos Santos, "Effective velocity distribution in an atom gravimeter: Effect of the convolution with the response of the detection," Phys. Rev. A: At., Mol., Opt. Phys. **90**(2), 023606 (2014).
4. J. Fang, J. G. Hu, X. Chen, H. R. Zhu, L. Zhou, J. Q. Zhong, J. Wang, and M. S. Zhan, "Realization of a compact one-seed laser system for atom interferometer-based gravimeters," Opt. Express **26**(2), 1586–1596 (2018).
5. Z. J. Fu, B. Wu, B. Cheng, Y. Zhou, K. X. Weng, D. Zhu, Z. Y. Wang, and Q. Lin, "A new type of compact gravimeter for long-term absolute gravity monitoring," Metrologia **56**(2), 025001 (2019).
6. S. K. Wang, Y. Zhao, W. Zhuang, T. C. Li, S. Q. Wu, J. Y. Feng, and C. J. Li, "Shift evaluation of the atomic gravimeter NIM-AGRb-1 and its comparison with FG5X," Metrologia **55**(3), 360–365 (2018).
7. Y. Bidel, N. Zahzam, C. Blanchard, A. Bonnin, M. Cadoret, A. Bresson, D. Rouxel, and M. F. Lequentrec-Lalancette, "Absolute marine gravimetry with matter-wave interferometry," Nat. Commun. **9**(1), 627 (2018).
8. P. W. Huang, B. Tang, X. Chen, J. Q. Zhong, Z. Y. Xiong, L. Zhou, J. Wang, and M. S. Zhan, "International Comparison of Absolute Gravimeters," Metrologia **56**(4), 045012 (2019).
9. X. J. Wu, Z. Pagel, B. S. Malek, T. H. Nguyen, F. Zi, D. S. Scheirer, and H. Müller, "Gravity surveys using a mobile atom interferometer," Sci. Adv. **5**(9), eaax0800 (2019).
10. M. J. Snadden, J. M. McGuirk, P. Bouyer, K. G. Haritos, and M. A. Kasevich, "Measurement of the Earth's Gravity Gradient with an Atom Interferometer-Based Gravity Gradiometer," Phys. Rev. Lett. **81**(5), 971–974 (1998).
11. F. Sorrentino, Q. Bodart, L. Cacciapuoti, Y. H. Lien, M. Prevedelli, G. Rosi, L. Salvi, and G. M. Tino, "Sensitivity limits of a Raman atom interferometer as a gravity gradiometer," Phys. Rev. A **89**(2), 023607 (2014).
12. Y. P. Wang, J. Q. Zhong, H. W. Song, L. Zhu, Y. M. Li, X. Chen, R. B. Li, J. Wang, and M. S. Zhan, "Location dependent Raman transition in gravity-gradient measurements using dual atom interferometers," Phys. Rev. A **95**(5), 053612 (2017).
13. R. Caldani, K. X. Weng, S. Merlet, and F. P. Dos Santos, "Simultaneous accurate determination of both gravity and its vertical gradient," Phys. Rev. A **99**(3), 033601 (2019).
14. D. K. Mao, X. B. Deng, H. Q. Luo, Y. Y. Xu, M. K. Zhou, X. C. Duan, and Z. K. Hu, "A dual-magneto-optical-trap atom gravity gradiometer for determining the Newtonian gravitational constant," Rev. Sci. Instrum. **92**(5), 053202 (2021).
15. D. S. Durfee, Y. K. Shaham, and M. A. Kasevich, "Long-term stability of an area-reversible atom-interferometer Sagnac gyroscope," Phys. Rev. Lett. **97**(24), 240801 (2006).
16. G. Tackmann, P. Berg, C. Schubert, S. Abend, M. Gilowski, W. Ertmer, and E. M. Rasel, "Self-alignment of a compact large-area atomic Sagnac interferometer," New J. Phys. **14**(1), 015002 (2012).
17. A. V. Rakholia, H. J. McGuinness, and G. W. Biedermann, "Dual-Axis High-Data-Rate Atom Interferometer via Cold Ensemble Exchange," Phys. Rev. A **2**(5), 054012 (2014).
18. Z. W. Yao, S. B. Lu, R. B. Li, J. Luo, J. Wang, and M. S. Zhan, "Calibration of atomic trajectories in a large-area dual-atom-interferometer gyroscope," Phys. Rev. A **97**(1), 013620 (2018).
19. D. Savoie, M. Altorio, B. Fang, L. A. Sidorenkov, R. Geiger, and A. Landragin, "Interleaved atom interferometry for high-sensitivity inertial measurements," Sci. Adv. **4**(12), eaau7948 (2018).
20. M. Altorio, L. A. Sidorenkov, R. Gautier, D. Savoie, A. Landragin, and R. Geiger, "Accurate trajectory alignment in cold-atom interferometers with separated laser beams," Phys. Rev. A **101**(3), 033606 (2020).
21. G. W. Biedermann, X. Wu, L. Deslauriers, S. Roy, C. Mahadeswaraswamy, and M. A. Kasevich, "Testing gravity with cold-atom interferometers," Phys. Rev. A **91**(3), 033629 (2015).
22. G. T. Foster, J. B. Fixler, J. M. McGuirk, and M. A. Kasevich, "Method of phase extraction between coupled atom interferometers using ellipse-specific fitting," Opt. Lett. **27**(11), 951–953 (2002).

Optics EXPRESS

23. W. J. Xu, L. Cheng, J. Liu, C. Zhang, K. Zhang, Y. Cheng, Z. Gao, L. S. Cao, X. C. Duan, M. K. Zhou, and Z. K. Hu, "Effects of wave-front tilt and air density fluctuations in a sensitive atom interferometry gyroscope," Opt. Express **28**(8), 12189–12200 (2020).